Research Article

Design and analysis of microfluidic cell counter using spice simulation

Sheikh Muhammad Asher Iqbal[1] · Nauman Zafar Butt[1]

Abstract
Microfluidic cytometers based on Coulter principle have recently shown a great potential for point of care biosensors for medical diagnostics. In this study, the design and characterization of Coulter-based microfluidic cytometer are investigated through electrical circuit simulations considering an equivalent electrical model for the biological cell. We explore the effects related to microelectrode dimensions, microfluidic detection volume, suspension medium, size/morphology of the target cells, and the impedance of the external readout circuit, on the output response of the sensor. We show that the effect of microelectrodes' surface area and the dielectric properties of the suspension medium should be carefully considered when characterizing the output response of the sensor. In particular, the area of the microelectrodes can have a significant effect on cell's electrical opacity (the ratio of cell impedance at high to low frequency) which is commonly used to distinguish between subpopulations of the target cells (e.g., lymphocytes vs. monocytes when counting white blood cells). Moreover, we highlight that the opacity response versus frequency can significantly vary based upon whether the absolute cell impedance or the differential output impedance is used in its calculation. These insights could provide valuable guidelines for the design and characterization of Coulter-based microfluidic sensors.

Keywords Microfluidic cell counter · Coulter principle · Electrical cell model

1 Introduction

The interaction of biological cells with an externally applied electrical field finds many applications in medical science [1]. For example, in the process of electroporation, stimulation of cells at a high electrostatic field is used to create pores in the cell membrane which allow for transferring drugs or DNA into the cell [2]. Similarly, in dielectrophoresis, forces exerted on the cell due to an applied AC electric field are used to separate cells having different size or shape. This technique finds various medical applications such as separating cancer cells from healthy cells, platelets from the whole blood, and live cells from dead cells. [3]. A relatively recent application of the electrical interaction of biological cells is in the area of medical diagnostics where microfluidic cell cytometry based on the Coulter principle is used to enumerate biomarkers for a particular disease [4]. Other applications of this technique include purification of liquids by detecting particles of impurities, detecting pollens, and drug administering. A typical Coulter-based cell cytometer can count or sort cells of various types based on the change in the electrical impedance of a ~ microliter volume of an electrolyte as the cells flow across the embedded microelectrodes. In an immunoassay biochip, two identical counters are typically placed, one at the inlet, and, the other at the outlet of a microfluidic immuno-capture chamber. The capture chamber contains antibodies that are specific to the target biomarkers and are usually coated on 3D micropillars to enhance the capture efficiency. A differential counting of the biomarker

Electronic supplementary material The online version of this article (https://doi.org/10.1007/s42452-019-1327-1) contains supplementary material, which is available to authorized users.

✉ Nauman Zafar Butt, nauman.butt@lums.edu.pk | [1]Department of Electrical Engineering, SBA School of Science and Engineering, Lahore University of Management Sciences (LUMS), Lahore, Pakistan.

SN Applied Sciences (2019) 1:1290 | https://doi.org/10.1007/s42452-019-1327-1

Received: 17 July 2019 / Accepted: 19 September 2019 / Published online: 26 September 2019

at the entry and the exit of the chamber is used to enumerate the target biomarker. An on-chip electronic circuit for signal processing and data acquisition can potentially be integrated with the microfluidic biochip for the portable biosensor. The main advantages of these electronic biochips are their high precision, label-free detection, portability, and compatibility with high-throughput chip-manufacturing process.

One of the prime applications of microfluidic cell cytometry is to detect biological cells which lead to diagnosis of fatal diseases like HIV/AIDS and Cancer. Currently, there are about 36.4 million people globally being affected by HIV/AIDS and their number is increasing at a rate of 5000 new infections per day [5]. Around 11 million (30%) of these HIV/AIDS patients did not have access to HIV testing services. A microfluidic point of care device could be extremely valuable for a low cost and accessible solution for such epidemics. In this regard, immunoassays based on Coulter-based microfluidic enumeration of biomarkers in a drop of blood sample have recently attracted a lot of attention for point of care (PoC) medical diagnostics [6, 7]. A variety of applications have been demonstrated including stratification of sepsis based on the real-time quantification of CD64 and cytokines, and, HIV/AIDS prognostics using CD4 enumeration [7].

Previously, Chen et al. [8] have summarized developments in microfluidic impedance-based cytometry in a chronological order. Gawad et al. [9] demonstrated an impedance spectrometry microfluidic cytometer for cell analysis and sorting. The study used 3D finite element simulation to compare different electrode geometries and cell positions. A simplified version of the electrical model for the biological cell was used that was originally introduced by Schoenbach et al. [10] to understand the impedance response of the sensor. Ellappan and Sundararajan [11] used Cadence Spectra tool to study the basic response of a biological cell at variable signal frequencies. Jayara et al. [12] optimized the microfluidic channel for the cell growth and described useful approaches to fabricate, optimize, and validate a biocompatible device. This work concluded that an increase in the channel depth could induce surface roughness which could significantly affect the device characteristics. Qiu et al. [13] optimized the microfluidic channel to improve the hydrodynamic dissociation of cells from tissues and organs for cell identification and disease diagnosis. Watkins et al. [6] developed a differential microfluidic cytometry technique for the $CD4^+$ and $CD8^+$ lymphocyte counter for HIV diagnostic applications. Hassan et al. [14] published detailed protocols for the fabrication of differential microfluidic cytometer biochip. Hassan et al. [15] demonstrated an application of the differential microfluidic cell counter biochip for the complete blood cell count. In another study [7], Hassan used the differential cell counter biochip to characterize CD 64 cells from the whole-blood samples for sepsis stratification. More recently, PoC microfluidic immunoassays based on Coulter principle have been applied to enumerate proteins in a drop of whole blood [16].

A number of other microfluidic platforms based on impedance cytometry have been demonstrated for the biodetection and analysis of micro-analytes. For example, Evander et al. [17] discriminated platelets from red blood cells using cellular electrochemical impedance spectroscopy and dielectrophoresis. Haandbaek et al. [18] characterized the subcellular morphology of yeast cell using a novel microfluidic impedance cytometer that is capable of simultaneous analysis at four frequencies between DC and 500 MHz. Haandbaek et al. [19] also detected single bacteria using microfluidic impedance cytometer by incorporating a series resonator circuit that improved the sensor's sensitivity. Song et al. [20] developed a noninvasive, label-free, micropore-based microfluidic impedance flow cytometer for the identification of the differentiation state of the stem cells. Bernabini et al. [21] demonstrated the detection of microparticles by hydrodynamically focusing the particles in the center of 200-µm microfluidic channel. The proposed technique demonstrated a high sensitivity for the microfluidic cytometer while maintaining large channel dimensions. Liu et al. [22] utilized electrical impedance differential sensing for the detection of sickle cells by combining it with oxygen control onto a single microfluidic chip. Petchakup et al. [23] developed a novel microfluidic strategy by combining the label-free leukocyte sorting with impedance profiling. With this technique, enhanced impedance detection selectivity for diabetes testing was demonstrated. Honrado et al. [24] characterized *plasmodium falciparum*-infected red blood and differentiated infected and non-infected red blood cells based on their cell membrane properties. Chawla et al. [25] demonstrated an integrated microfluidic platform that can be used to assess the viability of newly transformed schistosomula (NTS) using an impedance-based analysis method. The proposed platform was used for the automated antischistosomal drug screening. Chawla et al. [26] also used microfluidic platform for the long-term culturing and high-resolution imaging of yeast cells. Finally, the microfluidic cytometry has also been used for organ-on-chip applications, e.g., for cell detection with temporal regulation of the cell microenvironment [27], for selective detection of the migratory properties of cancer cells [28], and for measuring transepithelial electrical resistance (TEER) [29].

Although a large number of studies have demonstrated the application of microfluidic cytometer for a variety of biomarkers' detection, the design aspects of the cytometer and a systematic analysis of its

performance as a function of cellular properties and those of the suspension medium are relatively unexplored in the literature. In particular, a detailed study of the electrical characterization or modeling of the microfluidic cytometer system is desired which could guide the device design and help in the interpretation of experimental data. In this paper, we use electrical circuit simulations to investigate the design insights and guidelines for the optimized structural and circuit parameters of the device. In particular, we study the effects of microelectrode dimensions, medium's impedance and its dielectric properties, the readout circuit's resistance, and the dimensions of the microfluidic channel on the electrical output of the sensor. Moreover, we explore the electrical response of the sensor as a function of varying the cell properties such as cytoplasm and nuclear impedances and membrane capacitance. Finally, the electrical opacity for the cells which can provide useful information about cell membrane properties is discussed in context of the design parameters and the input signal frequency. Some of the unique contributions of our study are: (1) The effect of electrode area on the opacity. Moreover, the significance of the method for defining opacity in the experiments and the related effect of various cell/system parameters on opacity is discussed, (2) the effect of selecting the external readout resistance on the output signal is quantified, and (3) the effect of practical suspension mediums such as PBS, whole blood, DI water, on modifying the detection signal is presented.

2 Modeling approach

The detection of cell biomarker in a microfluidic counter is based on sensing the difference in the impedance inside a detection volume as the cell traverses through it. In the literature, the cell impedance in a suspension medium has been modeled through several approaches [30]. These include the finite element/difference methods [31], equivalent circuit model [32, 33], the boundary element method [34], and the transport lattice method [35, 36]. We have used the equivalent circuit model approach in this work. Although this approach is simpler as compared to other approaches, it can be very useful to highlight the qualitative trends important for the design and characterization of the device.

The equivalent circuit model is implemented in LT Spice (LTspice) which is a high-performance SPICE (Simulation Program with Integrated Circuit Emphasis) tool widely used for simulating electrical circuits. The output voltage signal from the microelectrode sensor is monitored as a function of broad range of physical design parameters for the applied electrical signal frequency ranging from 100 Hz to 100 MHz.

2.1 Cell electrical model

Figure 1a shows an illustration of a biological cell that consists of a cell membrane, cytoplasm and nucleus. An equivalent electrical model for the cell [10] is shown in Fig. 1b. The cell has been modeled as a uniform conductive medium, i.e., cytoplasm, having a nucleus and an outer cell membrane. The cell membrane has been modeled as a bilayer spherical

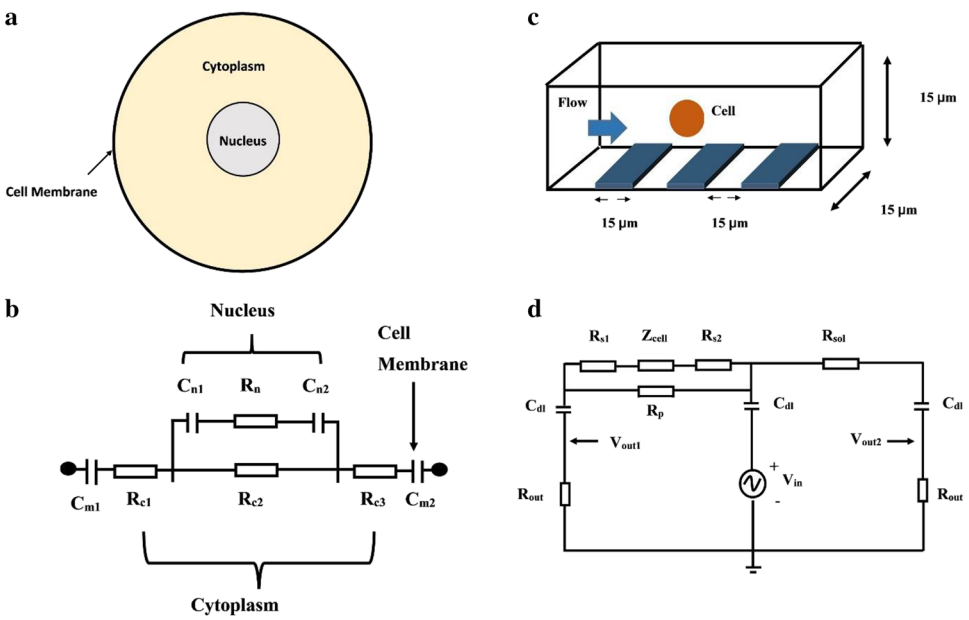

Fig. 1 **a** Illustration of a biological cell. **b** Electrical circuit model for the cell. **c** Illustration of cell flow through microelectrodes in the detection volume. **d** Overall electrical circuit for the cell counter

dielectric having capacitance, $C_m = \left(\frac{\kappa\varepsilon A}{d}\right)$. Nucleus of the cell is modeled as a double lipid bilayer having capacitance, C_n which is half of that of C_m. The cell's cytoplasm is modeled as a resistance, R_c. The impedance of the suspension medium (excluding cells) in the microfluidic detection volume is represented by the resistance of solution (R_{sol}). A double-layer capacitance C_{dl} appears at the interface between a conductive electrode and an adjacent liquid electrolyte [37]. We take the resistivity of cytoplasm and nuclear plasma to be the same and assume a typical value of 100 Ω cm [10]. For our reference cell diameter of 15 um, this gives $R_{c1} = 16.7\,\text{K}\Omega, R_{c2} = 133\,\text{K}\Omega, R_{c3} = 16.7\,\text{K}\Omega, C_m = 4$ pF,and, $C_n = 2$ pF. Finally, nuclear resistance is assumed to be equal to the cytoplasm resistance, i.e., $R_n = 133\,\text{K}\Omega$ (Eqs. 1–4). Perturbation to these reference values for cell parameters are specified when used. The amplitude (||) and phase ($\angle$) of the cell impedance, (Z_{cell}) as function of frequency (f) of the applied voltage are plotted in Fig. 2a. The detection volume is considered to be equal to the cell volume unless otherwise specified. Since amplitude of a capacitor's impedance scales inversely with frequency, $|Z_{cell}|$ decreases with increasing f until all of the capacitive elements in Z_{cell} becomes negligibly small (i.e., the capacitors behave like a short circuit). For $f > 100$ kHz, the amplitude of Z_{cell} saturates to a minimum value while its phase approaches to zero (a characteristic of a pure resistive circuit).

$$R_{c1} = R_{c3} = \frac{\rho \times L}{A} = \frac{100}{4 \times 15 \times 10^{-4}} \tag{1}$$

$$R_{c2} = \frac{\rho \times L}{A} = \frac{100}{7.5 \times 10^{-4}} \tag{2}$$

$$C_{m1} = C_{m2} = \left(\frac{9 \times 8.85 \times 10^{-12} \times 4 \times \pi \left(7.5 \times 10^{-6}\right)^2}{2 \times 7 \times 10^{-9}}\right) \tag{3}$$

$$C_{n1} = C_{n2} = \frac{C_{m1}}{2} \tag{4}$$

2.2 Device structure

Figure 1c shows an illustration of the microfluidic cell counter. The device contains three coplanar micro electrodes immersed in the microfluidic detection volume. An AC electrical voltage signal of 1 V amplitude is applied at the middle microelectrode, while voltages at the remaining two microelectrodes are detected. The readout circuit comprises of two identical external resistances (R_{out}), which form a Wheatstone bridge connection with the microfluidic impedances (Fig. 1d). The series resistors (R_{s1} and R_{s2}) and parallel resistor (R_p) in Fig. 1d represents the suspension medium resistances surrounding the cell in the detection volume. For an ideal case, the cell size is equal to the detection volume for which R_{s1} and R_{s2} are assumed zero while R_p is infinite.

2.3 Sensing principle

A microfluidic counter based on Coulter principle senses the cells or polystyrene beads coated with proteins individually as they flow through the microelectrodes in a microfluidic channel having detection volume close to the diameter of a single target cell (or bead). As a cell traverses through the detection volume, it induces an electrical pulse at the microelectrodes due to a difference in the impedance between the biological cell and that of the background electrolyte medium. This electrical pulse is sensed across R_{out}. A differential voltage (ΔV_{out}) is sensed at the output of the cell counter by taking the difference between V_{out1} (when detection volume contains a cell) and V_{out2} (when there is no cell in detection volume) measured across R_{out1} and R_{out2}, respectively:

$$|\Delta V_{out}| = |V_{out1}| - |V_{out2}| = |(|I_1 - I_2|)| \times R_{out} \tag{5}$$

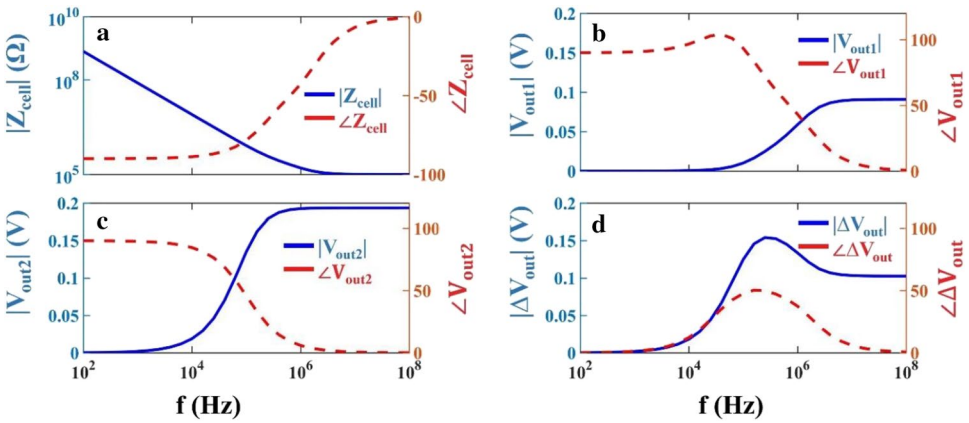

Fig. 2 **a** Cell impedance (amplitude and phase) versus frequency **b** V_{out1} (amplitude and phase) versus frequency, **c** V_{out2} (amplitude and phase) versus frequency **d** ΔV_{out} (amplitude and phase) versus frequency

where I_1 and I_2 are the AC electrical currents flowing out of left and right microelectrode, respectively. Figure 2b and 2c shows an example for the amplitude and phase of V_{out1} and V_{out2}, respectively. Since V_{out2} is influenced by C_{dl} and R_{sol} while V_{out1} is influenced by C_{dl} and Z_{cell}, their frequency response is different. In particular, V_{out2} for the given design shows saturation at a lower frequency as compared V_{out1}. Moreover, at high f (> 1 MHz), $Z_{cell} > R_{sol}$ for this device, so the saturated amplitude for V_{out2} is greater than that of V_{out1}. The resultant characteristics for ΔV_{out} are shown in Fig. 2d. From Fig. 2, it is evident that the design of device parameters (which influence C_{dl} and R_{sol}) and the cell's size/shape characteristics (which influence its capacitances and resistances) both can affect the sensor's output response. It should be noted that the frequency response of the sensor is significant for the cell analysis because the cell morphology (primarily the membrane capacitance) primarily affects ΔV_{out} at a specific range of frequency (typically around 1 MHz). The ratio between the output responses at a higher frequency to that at a lower frequency is therefore often used to extract valuable information about the cell shape and morphology [6, 9, 14]. This aspect is explored in detail in Sect. 3.

3 Results and discussion

In this section, the simulation and design of the microfluidic cytometer device is discussed in detail. The results and discussion are covered into four parts concerning: (1) device parameters that include microelectrode dimensions and R_{out}, (2) suspension medium parameters which includes its dielectric constant and R_{sol}, (3) microfluidic channel design parameters which includes the dimensions of the detection volume, and (iv) cell (biomarker) parameters which include electrical parameters related to its size/morphology.

3.1 Device parameters

Device parameters include optimizing electrode dimensions and external resistance, R_{out}.

3.1.1 Optimizing microelectrode dimensions

As the surface area (A) of the microelectrodes is directly proportional to C_{dl}, it can influence the output voltage response of the sensor. Figure 3a–c shows that the amplitude and phase of ΔV_{out} can both indeed be significantly modified with the change in A. As the electrode area increases, the amplitude of ΔV_{out} at lower frequencies is enhanced. Since all the capacitive impedances in the

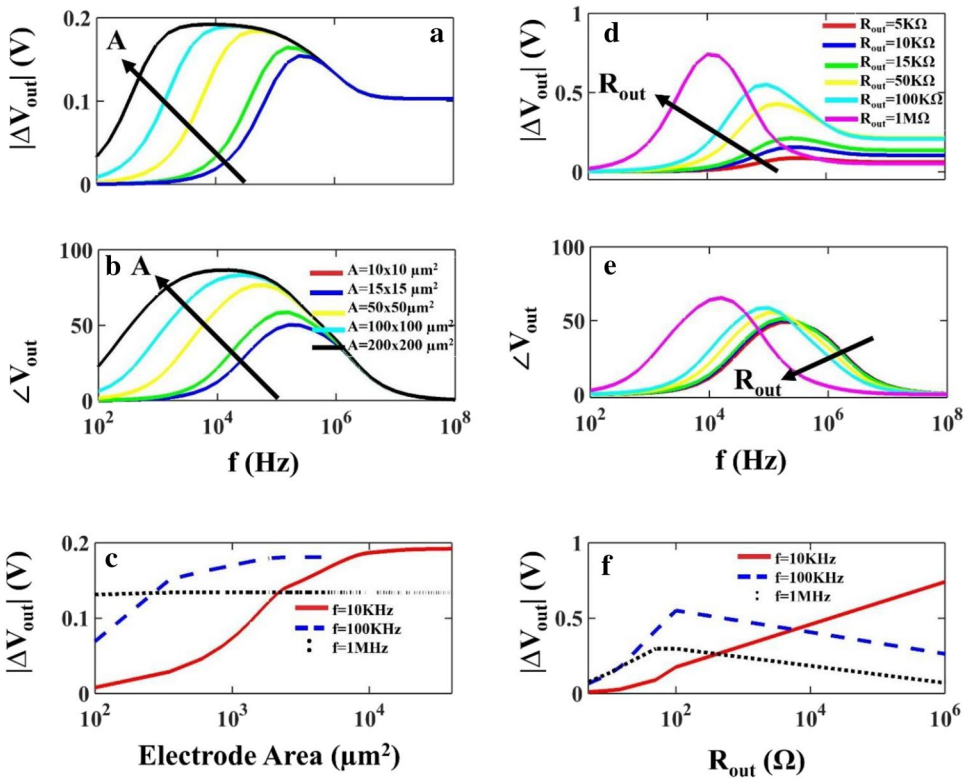

Fig. 3 **a** $|\Delta V_{out}|$ versus frequency for varying microelectrode area, **b** $\angle\Delta V_{out}$ versus frequency for varying microelectrode area, **c** $|\Delta V_{out}|$ versus microelectrode area at two different frequencies, **d** $|\Delta V_{out}|$ versus frequency for varying R_{out}, **e** $\angle\Delta V_{out}$ versus frequency for varying R_{out}, **f** $|\Delta V_{out}|$ versus R_{out} for different signal frequencies

circuit become negligible at high f (> 1 MHz), $|\Delta V_{out}|$ saturate to a constant amplitude which is determined by R_{sol} and the cell resistances. It can be noted that for the microelectrode area of $200 \times 200\ \mu m^2$, the low frequency peak of ΔV_{out} is most broad and high. For example, at $f = 10$ kHz, ΔV_{out} for $A = 200 \times 200\ \mu m^2$ and $A = 10 \times 10\ \mu m^2$ is 0.19 V and 0.7 mV, respectively, hence a shift of about 0.189 V. As f increases to ~ 1.5 MHz, $|\Delta V_{out}|$ saturates to a maximum of 0.1 V irrespective of A. Figure 3c shows $|\Delta V_{out}|$ as function of A for $f = 10$ kHz, 100 kHz, and, 1 MHz. While the microelectrode area has negligible effect on $|\Delta V_{out}|$ for f = 1 MHz, it significantly affects $|\Delta V_{out}|$ for f = 10 kHz It should be noted that an optimal value of A which can maximize the low frequency response of the sensor is slightly above $A = 10^4\ \mu m^2$. A further increase in A above this optimal value does not provide any additional benefit to the low frequency response of the sensor. Very small values (e.g., $< 10^3\ \mu m^2$), on the other hand, significantly degrade the sensor's output response for $f < 100$ kHz.

3.1.2 Optimizing R_{out}

Figure 3d–f shows ΔV_{out} trends with varying R_{out}. It should be noted that the choice of R_{out} not only influences $|\Delta V_{out}|$ at high frequency but could also affect the peak in the low frequency response. As R_{out} is increased above an initial value of 5 KΩ, $|\Delta V_{out}|$ both at high and low frequencies shows an increased amplitude. Increasing R_{out} above 50K, however, starts to saturate the amplitude of ΔV_{out} at high frequency but the low frequency response keeps showing an increase in amplitude. Finally, for $R_{out} = 100$ MΩ, the higher frequency amplitude significantly drops while the low frequency amplitude is further increased. From Fig. 3d, it is clear that an optimal choice of R_{out} for an impedance cytometer is significantly dependent on f. For example, at f = 100 kHz, an optimal R_{out} of 1 MΩ provides the largest amplitude for the output signal whereas at a higher frequency, i.e., 1 MHz, the optimal R_{out} is 50 KΩ. These results highlight that the choice of R_{out} must be made with consideration of the expected range of operating frequency of the cytometer.

3.2 Trends with suspension medium parameters

The suspension medium parameters include the resistance (R_{sol}) and dielectric constant (κ).

3.2.1 Resistance of the suspension medium

In a practical implementation of the microfluidic cytometer, the cells are counted directly from a lysed blood sample or blood plasma. Other reagents such as phosphate buffer solution (PBS) and deionized water (DI) can sometimes be incorporated as suspension medium for cells or beads in the laboratory characterization. The value of R_{sol} can be calculated from the conductivity of the solution medium for a given dimension of the detection volume [38]. Figure 4 shows the effect of R_{sol} on ΔV_{out}. It can been seen that highest ΔV_{out} is obtained when PBS 10× is the medium due to its high conductivity 12.3 S/m [39, 40]. For a phosphate-buffered solution (PBS 10×) medium (conductivity of 1.6 S/m) and the whole-blood sample having conductivity of 1.09 S/m [41, 42], ΔV_{out} at frequency 1 MHz is approximately 80 mV and 134 mV, respectively. For DI water solution, conductivity (5.5 × S/m) [43], is very low and results in a significant drop in ΔV_{out}.

3.2.2 Trends with dielectric constant

The dielectric properties of the solution medium affect C_{dl} and hence the electrical response of the cytometer. Figure 5a shows the plot between ΔV_{out} and the dielectric constants of different electrolyte solutions assuming $A = 15 \times 15\ \mu m^2$.

Figure 5a shows that the effect of increasing κ improves the low frequency amplitude of the cytometer output. This trend is similar to what is shown in Fig. 3a for ΔV_{out} response as a function of A. This is expected since both A and κ has as similar effect on the C_{dl} at all frequencies of the applied signal. Figure 5 shows that the effect of κ on ΔV_{out} is more drastic when $\kappa < 10$ for $f = 1$ MΩ, while for $f = 100$ KΩ, effect on ΔV_{out} for $\kappa > 10$ is more drastic. For smaller f(10 KΩ), variation of κ has a negligible effect on ΔV_{out}.

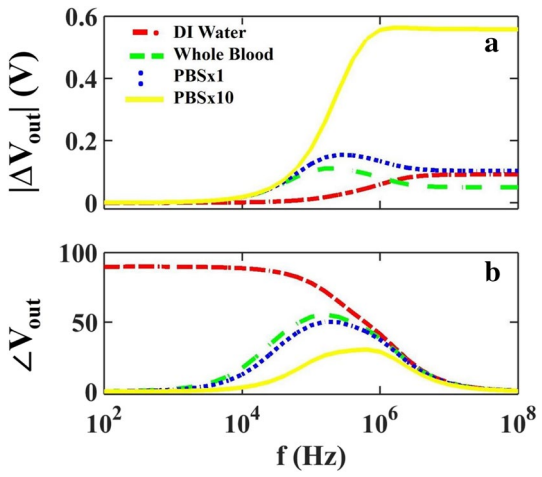

Fig. 4 **a** $|\Delta V_{out}|$ versus frequency for different suspension medium, **b** $\angle\Delta V_{out}$ versus frequency for different suspension medium

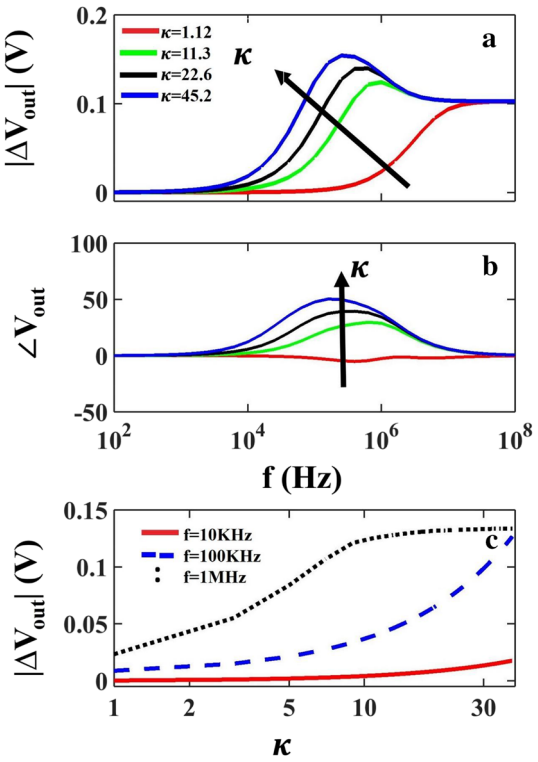

Fig. 5 **a** $|\Delta V_{out}|$ versus frequency for varying κ, **b** $\angle\Delta V_{out}$ versus frequency for varying κ, **c** $|\Delta V_{out}|$ versus κ at different signal frequencies

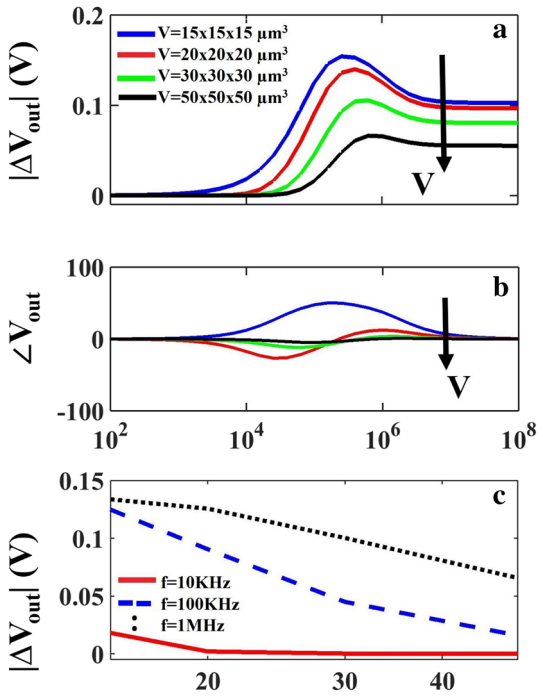

Fig. 6 **a** $|\Delta V_{out}|$ versus frequency for varying detection volume, **b** $\angle\Delta V_{out}$ versus frequency for varying detection volume, **c** $|\Delta V_{out}|$ as a function of detection volume for variable frequencies

3.3 Trends with channel dimensions

The analysis shown so far has assumed an ideal case where the cell volume is identical to the detection volume. This is although desirable but in practice may not be possible to implement due to variable cell size distribution of the target cells. Though the qualitative trends for ΔV_{out} are expected to be the same, the structural non-idealities could affect the cytometer's output signal. These structural non-idealities are incorporated as resistances in parallel (R_p) and series (R_s) as shown in Fig. 1d. For calculating V_{out1}, we have assumed that the cell is positioned exactly in the middle of the detection volume.

In Fig. 6a, $|\Delta V_{out}|$ for a target cell of 15 μm diameter are shown as the detection volume is varied from $15 \times 15 \times 15\,\mu m^3$ (ideal case) to $50 \times 50 \times 50\,\mu m^3$. The maximum $|\Delta V_{out}|$ is obtained for the ideal case, while a decrease in $|\Delta V_{out}|$ is observed as detection volume is increased. This is expected because a non-ideal detection volume adds additional current paths between the microelectrodes other than that through the cell thereby decreasing the electric field intensity across the cell and hence the ΔV_{out}.

3.4 Effect of cell parameters

The analysis done so far has been done without varying the cell impedances shown in the cell model (Fig. 1). In practice, however, the cell impedances may vary across a wide range based on the size, type, and morphology of the cell. For example, for complete blood counting (CBC) test, a microfluidic cytometer needs to simultaneously enumerate red blood cells (RBCs), white blood cells (WBCs), and platelets, etc. [15]. Moreover, the subpopulations of lymphocyte, granulocytes, and monocytes in WBC can be separated out from the electrical characteristics. In such experiments, ΔV_{out} and electrical opacity from microfluidic cytometers have often been used to distinguish between various types of blood cells as well as the subpopulations of the cells. In this section, we explore ΔV_{out} and opacity characteristics as a function of varying the morphology and size of the target cells.

For a given size of the cell, the morphological variations may change C_m and C_n without substantially affecting the cell resistances. Figure 7 shows the ΔV_{out} characteristics for varying the cell capacitances for two different microelectrode areas ($A_1 = 15 \times 15\,\mu m^2$ and $A_2 = 200 \times 200\,\mu m^2$) keeping all other cell/device parameters constant. For A_1, the effect of C_m is significant in range of f between 0.1 and 4 MHz. For A_2, however, the effect of varying C_m is significant in a range of $f = 2.5$ KHz $-$ 4 MHz. Figure 7e, f shows

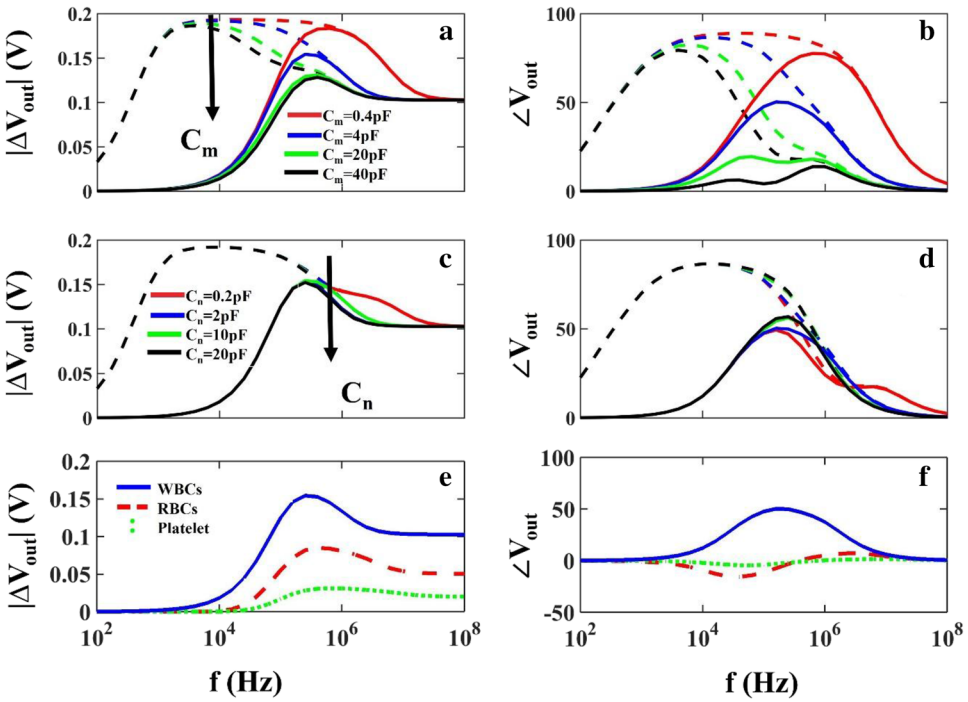

Fig. 7 **a** $|\Delta V_{out}|$ for varying cell membrane, C_m, **b** $\angle\Delta V_{out}$ for varying cell membrane, C_m, **c** $|\Delta V_{out}|$ for varying nuclear membrane, C_n, **d** $\angle\Delta V_{out}$ for varying nuclear membrane, C_n, **e** $|\Delta V_{out}|$ for different cell types, **f** $\angle\Delta V_{out}$ for different cell types

the ΔV_{out} characteristics for WBC (15 µm), RBS (6 µm), and, platelets (3 µm) keeping $A = 15 \times 15\ \mu m^2$. Here, since the cell size is varying, cytoplasm, and nuclear resistances are also changed accordingly along with the cell capacitances. Due to change in cell resistances, the high frequency ($f > 1$ MHz) response for $|\Delta V_{out}|$ also gets modified as observed in Fig. 7e.

Figure 8 shows modulation in cell opacity (OP) for cell capacitance variations (Fig. 8a–f) and for varying cell size (Fig. 8g–i). Two different approaches to define OP are compared in the three columns of Fig. 8. OP1 is defined as $\frac{V_{out1}(LF)}{V_{out1}(HF)}$ while OP2 is defined as $\frac{\Delta V_{out}(LF)}{\Delta V_{out}(HF)}$ where HF is the high frequency which is kept constant at 1 MHz and LF is the low frequency that is varied in Fig. 8. For OP1, that is shown in the leftmost column (Fig. 8a, d, g) the effect of C_{dl} is not substantial which results in OP1 being independent of the microelectrode area. For OP2, on the other hand, which shown in the middle column (Fig. 8b, c, e) for $A = 15 \times 15\ \mu m^2$, and in the rightmost column (Fig. 8f, h, i) for $A_2 = 200 \times 200\ \mu m^2$, the effect of C_{dl} is significant and therefore a prominent effect of the microelectrode area can be observed. Since opacity is often used to distinguish cell populations on the basis of membrane properties (irrespective of cell size), the effect

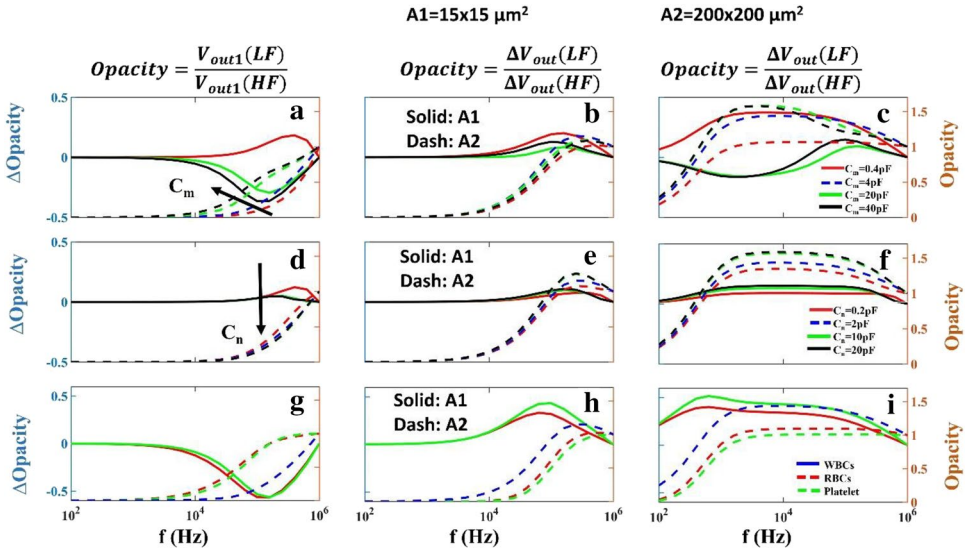

Fig. 8 Opacity and ΔOpacity as a function of the low frequency for: **a**–**c** Varying C_m, **d**–**f** Varying C_n **g**–**i** Varying cell types. For the left column (**a**, **d**, **h**), opacity is evaluated using the ratio of the absolute change in the cell impedance at low versus high frequency, while the ratio of differential impedance at low versus high frequency is used for middle (**b**, **e**, **h**) and right (**c**, **f**, **i**) columns. The middle and right columns use different areas for the microelectrodes

of microelectrode dimensions should be carefully considered when the differential voltage (impedance) signal from the cytometer readout circuit are used to calculate opacity. The most significant effect on OP is observed for varying C_m (Fig. 8a–c) while the variation in C_n shows a minor effect on OP.

4 Conclusions

The physical properties of the target biomarker and the structural design of the microfluidic counter have significant effect on the output response of the Coulter microfluidic cytometer. We have used circuit simulations based on equivalent cell model to quantify the impact of various design parameters for the device and the target cell characteristics on the output response of the device. The physical dimensions of the microelectrodes can strongly influence the output response of the sensor as a function of the frequency of the applied electrical stimulus. In particular, the lower frequency response can be significantly modulated with increasing microelectrode surface area due to the effect of double-layer capacitance. This trend is shown to saturate at microelectrode area close to $200 \times 200\,\mu m^2$. The detection volume should ideally be close to the size of the target cell to maximize the sensitivity. A detection volume bigger than the target cell size lowers the amplitude of higher frequency response while lower frequency response is less affected. The dielectric properties of the suspension medium and its electrical impedance can affect the lower and higher frequency response of the counter respectively. The resistance of the readout bridge circuit should be optimally selected based on the choice of the operating frequency. The cell's electrical opacity responds to the modulation in membrane capacitance for a specific range of signal frequencies that can strongly vary as a function of the microelectrode area and the choice of absolute cell impedance versus the differential output impedance for opacity calculation. With optimally designed device structure, a microfluidic counter can effectively sense the target cells at signal frequency as low as few KHz. These insights can provide valuable guidelines for the design and characterization of Coulter-based microfluidic sensors.

Funding This study was funded by Technology Development Fund (TDF02-127) from Higher Education Commission of Pakistan and Faculty Initiative Fund (FIF-414) from Lahore University of Management Sciences, LUMS.

Compliance with ethical standards

Conflict of interest Authors of this study have no conflicts of interest to declare.

References

1. Khine M, Lau A, Ionescu-Zanetti C, Seo J, Lee L (2004). https://doi.org/10.1039/b408352k
2. Gehl J (2003). https://doi.org/10.1046/j.1365-201X.2003.01093.x
3. Pethigand R, Markx GH (1997). https://doi.org/10.1016/S0167-7799(97)01096-2
4. Sun T, Morgan H (2010) Single-cell microfluidic impedance cytometry: a review. Microfluid Nanofluid 8(4):423–443
5. HIV.Gov. (2018). https://www.hiv.gov/hiv-basics/overview/data-and-trends/global-statistics
6. Watkins N, Hassan U, Damhorst G, Ni H, Vaid A, Rodriguez W, Bashir R (2013) Sci Transl Med. https://doi.org/10.1126/scitranslmed.3006870
7. Hassan U, Ghonge T, Reddy B Jr, Patel M, Rappleye M, Taneja I, Tanna A, Healey R, Manusry N, Price Z, Jensen T, Berger J, Hasnain A, Flaugher E, Liu S, Davis B, Kumar J, White K, Bashir R (2017). https://doi.org/10.1038/ncomms15949. www.nature.com/naturecommunications
8. Chen J, Xue C, Zhao Y, Chen D, Wu M, Wang J (2015) Microfluidic impedance flow cytometry enabling high-throughput single-cell electrical property characterization. Int J Mol Sci 16:9804–9830. https://doi.org/10.3390/ijms16059804
9. Gawad S, Schildb L, Renauda P (2001) Micromachined impedance spectroscopy flow cytometer for cell analysis and particle sizing. Lab on a Chip 1:76–82. https://pubs.rsc.org/en/content/articlepdf/2001/lc/b103933b. https://doi.org/10.1039/b103933b
10. Schoenbach K, Katsuki S, Stark R, Buescher E, Beebe S (2002) Bioelectrics-new applications for pulsed power technology. IEEE Trans Plasma Sci 30(1):293–300. https://doi.org/10.1109/TPS.2002.1003873
11. Ellappan P, Sundararajan R (2005) A simulation study of the electrical model of a biological cell. J Electrost 63:297–307. https://doi.org/10.1016/j.elstat.2004.11.007
12. Vibha J, Pramod W, Sameer J (2013) IEEE International nanoelectronics conference 978-1-4673-4842-3
13. Qiu X, Huang J, Westerhof T, Haun J (2018) Microfuidic channel optimization to improve hydrodynamic dissociation of cell aggregates and tissue. Nature. https://doi.org/10.1038/s41598-018-20931-y
14. Hassan U, Watkins N, Reddy B, Damhorst G, Bashir R (2016) Microfluidic differential immunocapture biochip for specific leukocyte counting. Protocol. https://doi.org/10.1038/nprot.2016.038
15. Hassan U, Reddy B, Damhorst G, Sonoiki O, Ghonge T, Yang C, Bashir R (2015) A microfluidic biochip for complete blood cell counts at the point-of-care. Technology 3(4):201–213. https://doi.org/10.1142/S2339547815500090
16. Valera E, Berger J, Hassan U, Ghonge T, Liu J, Rappleye M, Winter J, Abboud D, Haidry Z, Healey R, Hung NT, Leung N, Mansury N, Hasnain A, Lannon C, Price Z, White K, Bashir R (2018) A microfluidic biochip platform for electrical quantification of proteins. Lab Chip 18(10):1461–1470. https://doi.org/10.1039/c8lc00033f
17. Evander M, Ricco AJ, Morser J, Kovacs GT, Leung LL, Giovangrandi L (2013) Microfluidic impedance cytometer for platelet analysis. Lab Chip 13(4):722–729

18. Haandbæk N, Bürgel SC, Heer F, Hierlemann A (2014) Characterization of subcellular morphology of single yeast cells using high frequency microfluidic impedance cytometer. Lab Chip 14(2):369–377
19. Haandbæk N, Bürgel SC, Heer F, Hierlemann A (2014) Resonance-enhanced microfluidic impedance cytometer for detection of single bacteria. Lab Chip 14(17):3313–3324
20. Song H, Wang Y, Rosano JM, Prabhakarpandian B, Garson C, Pant K, Lai E (2013) A microfluidic impedance flow cytometer for identification of differentiation state of stem cells. Lab Chip 13(12):2300–2310
21. Bernabini C, Holmes D, Morgan H (2011) Micro-impedance cytometry for detection and analysis of micron-sized particles and bacteria. Lab Chip 11(3):407–412
22. Liu J, Qiang Y, Alvarez O, Du E (2018) Electrical impedance microflow cytometry with oxygen control for detection of sickle cells. Sens Actuators B Chem 255:2392–2398
23. Petchakup C, Tay HM, Yeap WH, Dalan R, Wong SC, Li KHH, Hou HW (2018) Label-free leukocyte sorting and impedance-based profiling for diabetes testing. Biosens Bioelectron 118:195–203
24. Honrado C, Ciuffreda L, Spencer D, Ranford-Cartwright L, Morgan H (2018) Dielectric characterization of *Plasmodium falciparum*-infected red blood cells using microfluidic impedance cytometry. J R Soc Interface 15(147):20180416
25. Chawla K, Modena MM, Ravaynia PS, Lombardo FC, Leonhardt M, Panic G, Bürgel SC, Keiser J, Hierlemann A (2018) Impedance-based microfluidic assay for automated antischistosomal drug screening. ACS Sens 3(12):2613–2620
26. Chawla K, Bürgel SC, Schmidt GW, Kaltenbach HM, Rudolf F, Frey O, Hierlemann A (2018) Integrating impedance-based growth-rate monitoring into a microfluidic cell culture platform for live-cell microscopy. Microsyst Nanoeng 4(1):8
27. Sart S, Tomasi RFX, Amselem G, Baroud CN (2017) Multiscale cytometry and regulation of 3D cell cultures on a chip. Nat Commun 8(1):469
28. Nguyen TA, Yin TI, Reyes D, Urban GA (2013) Microfluidic chip with integrated electrical cell-impedance sensing for monitoring single cancer cell migration in three-dimensional matrixes. Anal Chem 85(22):11068–11076
29. Van der Helm MW, Odijk M, Frimat JP, van der Meer AD, Eijkel JC, van den Berg A, Segerink LI (2017) Fabrication and validation of an organ-on-chip system with integrated electrodes to directly quantify transendothelial electrical resistance. JoVE 127:e56334
30. Morgan H, Sun T, Holmes D, Gawad S, Green N (2006) Single cell dielectric spectroscopy. J Phys D Appl Phys 40(1):61
31. Asami K (2006) Dielectric dispersion in biological cells of complex geometry simulated by the three-dimensional finite difference method. J Phys D Appl Phys 39(3):492
32. Foster KR, Schwan H (1989) Dielectric properties of tissues and biological materials: a critical review. Crit Rev Biomed Eng 17:25–104
33. Gimsa J, Wachner D (1998) A unified resistor-capacitor model for impedance, dielectrophoresis, electrorotation and induced transmembrane potential. Biophys J 75:1107–1116
34. Sekine K (2000) Application of boundary element method to calculation of the complex permittivity of suspensions of cells in shape of D∞h symmetry. Bioelectrochemistry 52:1–7
35. Gowrishankar TR, Weaver JC (2003) An approach to electrical modeling of single and multiple cells. Proc Natl Acad Sci USA 100:3203–3208
36. Stewart DA, Gowrishankar TR, Smith KC, Weaver JC (2005) Cylindrical cell membranes in uniform applied electric fields: validation of a transport lattice method. IEEE Trans Biomed Eng 10:1643–1653
37. Hou Y. Controlling variables of electric double-layer capacitance. https://core.ac.uk/download/pdf/61363805.pdf. Accessed 23 Oct 2018
38. Gawad S, Cheung K, Seger U, Bertsch A, Renaud P (2004) Dielectric spectroscopy in a micromachined flow cytometer: theoretical and practical considerations. Lab Chip 4:241–251
39. Lenntech (2018) Water treatment and purification. https://www.lenntech.com/
40. https://www.lenntech.com/applications/ultrapure/conductivity/water-conductivity.htm
41. Schwan H (1998) Electroporation and electrofusion in cell biology, 1st edn. Plenum Press, New York, pp 3–21
42. Schwan H, Takashima S, Miyamoto V, Stoeckenius E. https://doi.org/10.1016/s0302-4598(00)00072-6
43. http://www.myronl.com/PDF/application_bulletins/di_ab.pdf